

Effects of Stirring Time on Formation of Microplastics Fragmented from Photo-aged Polypropylene

*Kazuya Haremaki^a, Takumitsu Kida^b, Yusuke Koide^a,
Takashi Uneyama^a, Yuichi Masubuchi^a, Takato Ishida^{a*}*

^a Department of Materials Physics, Nagoya University, Furo-cho, Chikusa, Nagoya 464-8603, Japan

^b Department of Materials Chemistry, Faculty of Engineering, The University of Shiga Prefecture, 2500, Hassaka, Hikone, 522-8533, Japan

* E-mail: ishida@mp.pse.nagoya-u.ac.jp

ABSTRACT

This paper examines the evolution of microplastic (MP) size distributions fragmented from photo-aged polypropylene (PP) in stirred water. PP specimens fragmented into MPs with their size of 1–30 μm after UV irradiation and stirring in laboratory settings. MPs were dispersed into the water during the stirring process. A series of MP size distributions was analyzed from optical microscope images of obtained MPs. The MP size distribution was described by an exponential function in the short stirring time domain, whereas it changed to a power-law function as the stirring time increased. The fragmentation rate of MPs and nanoplastics (NPs) decreased with increasing stirring time. The obtained MP exhibited higher crystallinity than the photo-aged PP specimen after stirring. This result implies that MP fragmentation is induced by the chemicrystallization of PP.

KEY WORDS

1. INTRODUCTION

Microplastics (MPs) are tiny plastic particles whose size ranges from 1 μm to 5 mm [1]. As reported, MPs are fragmented from plastic debris. MPs are found in various environments on the Earth, starting from in soils to the atmosphere [2–7]. They are also found in biological environments such as inside human bodies [8,9]. The most major environment where MPs are commonly found is the ocean. The presence of MPs in the marine environment has become a serious problem today. The size of MPs affects transport and fragmentation process in the ocean [10,11]. It is important to reduce the fragmentation of MPs with specific sizes, which are harmful to the marine environment. Elucidating the mechanisms of MP fragmentation and identifying key factors that induce fragmentation are crucial.

Halle et al. [11] proposed a widely accepted scenario for MP fragmentation from plastic waste in marine environments: (i) embrittlement caused by photo-oxidative degradation, followed by (ii) MP formation under mechanical stress. In the polyolefin family, a major source of MPs, oxidation leads to chain scission in the amorphous region. This process also induces chemi-crystallization and embrittlement [12–14]. In severely aged samples, it has been known since the 1980s that chemi-crystallization induces internal stress distribution, and the stress inhomogeneity is released through the spontaneous formation of orthogonal surface cracks [15,16]. MPs are fragmented when mechanical stress causes fragmentation of the embrittled surface, and the crack edges [17]. In the marine environment, marine plastic debris experiences mechanical stresses that originate from various stimuli such as waves, wind, sand collisions, and interactions with marine organisms [18,19].

Several studies have reported statistical analyses of the size distribution of MPs collected from both the environment and laboratory tests. Various reports indicate that the size distribution follows a power-law distribution [11,17,20–26]. A simple analytic model is proposed to explain this power-law behavior. It claims that the power-law with the exponent of 3 is realized, assuming that cubic elements undergo a cascading fragmentation process [23]. However, some previous studies showed

that the power-law exponent is yet uncertain [20–22], probably due to some differences in fragmentation conditions and the MP size range observed in each study. Another possible reason is the lack of studies that consider the time evolution of MP fragmentation behavior.

In this study, photo-aged polypropylene (PP) specimens with a fixed oxidative aging treatment were prepared and stirred in water to fragment MPs, and the time evolution of the MP size distribution was investigated. The fragmented specimens were observed by optical microscopy, Raman spectroscopy, infrared (IR) spectroscopy, and differential scanning calorimetry (DSC). The results showed that (i) the size distribution changed from exponential to power-law distribution as the string time increased and that (ii) high crystallinity regions are preferentially fragmented into MPs. Details are shown below.

2. EXPERIMENTAL

2.1 Materials and Specimens Preparation

The isotactic polypropylene (PP) used in this study was obtained from Sigma-Aldrich (molecular weight $M_w = 3.5 \times 10^5$, and $M_w/M_n = 3.6$). The supplied pellets of PP were placed between two 100 μm -thick and 150 mm \times 150 mm aluminum sheets coated with polyimide films, together with a 1 mm-thick and 150 mm \times 150 mm aluminum spacer featuring a 100 mm \times 100 mm square cut-out. PP was molded at 200 °C and 15 MPa for 15 minutes by a test press (MP-2FH, Toyo-Seiki). The pressed sheets were then cooled gradually to room temperature. The obtained sheets were cut into 10 mm \times 10 mm specimens.

2.2 Photo-aging

The photo-aging treatment was conducted under an OPM2-502XQ xenon lamp (USHIO Inc., Japan) while the 10 mm \times 10 mm specimens were placed on a house-made hot plate of which temperature was controlled to be 70 °C. The mirror mounted on the lamp ensured horizontal irradiation for the specimen. The average UV radiation flux density was 6.54 mW/cm² at 365 nm, measured by UIT-250 accumulated UV meter (USHIO Inc., Japan), with UVD-S365 photodetector

(USHIO Inc., Japan).

2.3 Fragmentation

A single photo-aged specimen was placed in a 30 mL screw tube vial (60 mm height, 30 mm diameter) containing 15 mL of distilled water and stirred using a VTX-3000L vortex mixer (LMS Co. Ltd., Japan) at 500 rpm for up to 400 h to fragment MPs. Throughout the stirring process, the remaining specimen was periodically removed from the vial and transferred to a new vial containing fresh 15 mL deionized water at 5, 10, 20, 50, 100, 200, and 400 h of stirring. After transferring the specimens, the water remaining in the vial, including MPs, at each stirring period (0–5 h, 5–10 h, 10–20 h, 20–50 h, 50–100 h, 100–200 h, and 200–400 h) was obtained. Because the MP fragmentation rate would decrease with time, the period between transfers was increased as the stirring time increased.

2.4 Characterization of The Remaining PP Specimen

At each transfer between vials, the PP specimen was analyzed as follows. The surface was observed by a polarizing optical microscope (BX53, OLYMPUS, Japan) that was equipped with a crossed polarizer and a retardation plate. Reflection illumination was employed for observations of the specimen photo-aged and stirred for 400 h after photo-aging, with a spatial resolution of the imaging was 0.22 $\mu\text{m}/\text{pixel}$. Transmission illumination was employed for observations of the unaged specimen sliced by a microtome (THK, KENIS Ltd., Japan), with a spatial resolution of the imaging was 0.11 $\mu\text{m}/\text{pixel}$.

The infrared (IR) spectra were taken by Nicolet iS10 FT-IR spectrometer (Thermo Fisher Scientific, USA). Attenuated total reflection (ATR) measurements were performed with an ATR accessory (ATR ITX BASE, Thermo Fisher Scientific, USA) and a diamond crystal (ATR ID7/ITX noncoated diamond crystal, Specac Ltd, Britain). All IR spectra were collected over a range of 4000–400 cm^{-1} with a resolution of 1 cm^{-1} , and each spectrum was averaged over 64 scans.

DSC analysis was conducted with a Discovery DSC 25 (TA Instruments, USA) over a temperature range from 50 °C to 200 °C at a heating rate of 10 °C/min under a nitrogen atmosphere. The samples were sealed in a closed pan to prevent the loss of volatile components.

After photo-aging and stirring, Raman spectroscopy of PP specimens and MP was conducted using inVia Reflex Raman micrometer (Renishaw, UK) with a green laser (wavelength: 532 nm, power: 50 mW) and an objective lens $\times 100$. Each Raman spectrum was accumulated 32 times with an exposure time of 2 s under a non-polarized condition by inserting a $1/4$ wavelength filter in the incident-light path. All Raman spectra were collected over a range of $1800\text{--}5\text{ cm}^{-1}$ with a resolution of 2 cm^{-1} .

Mapping measurement of the orientation of unaged PP specimen was conducted using inVia Reflex Raman micrometer (Renishaw, UK) with an objective lens $\times 100$ on a selected area of $150\text{ }\mu\text{m}\times 150\text{ }\mu\text{m}$ with a step size of $3\text{ }\mu\text{m}$. Each Raman spectrum was obtained over a range of $1800\text{--}5\text{ cm}^{-1}$ with a resolution of 2 cm^{-1} under hh polarization, where the polarization direction of the incident light was parallel to the scattered light, with an exposure time of 0.2 s. The intensity ratio of the Raman band at 973 and 998 cm^{-1} is used as an orientation parameter $R = A_{975}/A_{998}$. The higher value of R indicates that the crystalline chains orient to the polarization direction [27].

2.5 MP Size Distribution Measurements

After the removal of the specimen during the fragmentation process, to obtain MP size distribution at each stirring period, the remaining water containing MPs was processed as follows. The liquid was partially dried in AVO-310NB vacuum oven (AS ONE Co., Japan) at $70\text{ }^{\circ}\text{C}$ in order to increase the MPs concentration. A single drop of the concentrated MPs dispersion was sampled with a glass rod and transferred to a slide glass. Afterward, the water on the slide glass was fully evaporated. Polarized optical microscope images of MPs on the slide glass were taken by the microscope mentioned in section 2.4, under a transmission illumination. The spatial resolution of the imaging was $0.11\text{ }\mu\text{m}/\text{pixel}$. The acquired images were processed by ImageJ2 (version 2.14.0). The hue channel was

binarized, and Feret's diameters of MP particles were measured. The Feret's diameter corresponds to the maximum size measured by the caliper. The MP size, defined as the Feret's diameter, was measured for at least 1000 MP particles. Then, the MP size distributions were organized as histograms with a bin size of 1 μm . The MP particles smaller than 1 μm were excluded from the size distributions.

2.6 MP Fraction Measurements

Apart from the MP size distribution measurement, the amount of fragmented MPs and nanoplastics (NPs) at each stirring period was determined as follows. The concentrated MP dispersion, prepared in section 2.5, was completely evaporated in an AVO-310NB vacuum oven (AS ONE Co., Japan) at 70 $^{\circ}\text{C}$. The remaining MPs and NPs in the vial were then diluted with about 3 mL acetone as a solvent. The acetone solution containing MPs and NPs was transferred to a 5 mL glass syringe and dripped at a constant rate of 2.00 mL/h into an aluminum DSC pan with an MSP-1D syringe pump (AS ONE Co., Japan). The temperature of the DSC pan was kept at 50 $^{\circ}\text{C}$ by the house-made hot plate in order to quickly evaporate the solvent. To collect MPs remaining in the vial, acetone was added to the vial again and the same procedure was iterated more than three times to reduce the loss of MPs as much as possible. In order to evaporate the solvent completely, the DSC pan was dried in an AVO-310NB vacuum oven (AS ONE Co., Japan) at 60 $^{\circ}\text{C}$ for 12 h.

The change in weight of the pan is regarded as the weight of fragmented MPs and NPs. The accumulated weight of fragmented MPs and NPs was calculated as the sum of the measured weights:

$$W_{\text{frag},n} = \sum_{i=1}^n w_{\text{frag},i} \cdot \quad (1)$$

Here, $w_{\text{frag},i}$ represents the weight of MPs and NPs fragmented during the i -th stirring period, and $W_{\text{frag},i}$ is the accumulated weight up to the i -th stirring period. The average fragmentation rate of MPs and NPs during the i -th stirring period is defined as follows:

$$R_{\text{frag},i} = \frac{w_{\text{frag},i}}{t_i - t_{i-1}}, \quad (2)$$

where t_i is the end of the i -th stirring period (i.e., 5 h, 10 h, 20 h, 50 h, 100 h, 200 h, and 400 h).

3. RESULTS

3.1 Observation of MPs by Polarized Optical Microscopy

Figure 1 shows polarized optical microscope images of fragmented MPs at each stirring period (20–50 h, 50–100 h, 100–200 h, and 200–400 h). Some waxy residues, not identified as MPs, were observed during the early stage (up to 20 h). The size of the MPs ranges from larger than 1 μm to smaller than 30 μm , with various shapes, consistent with the earlier studies [28–32]. The size of MPs fragmented before 200 h of stirring did not appear to differ significantly from each other, whereas larger MPs were fragmented after 200 h of stirring.

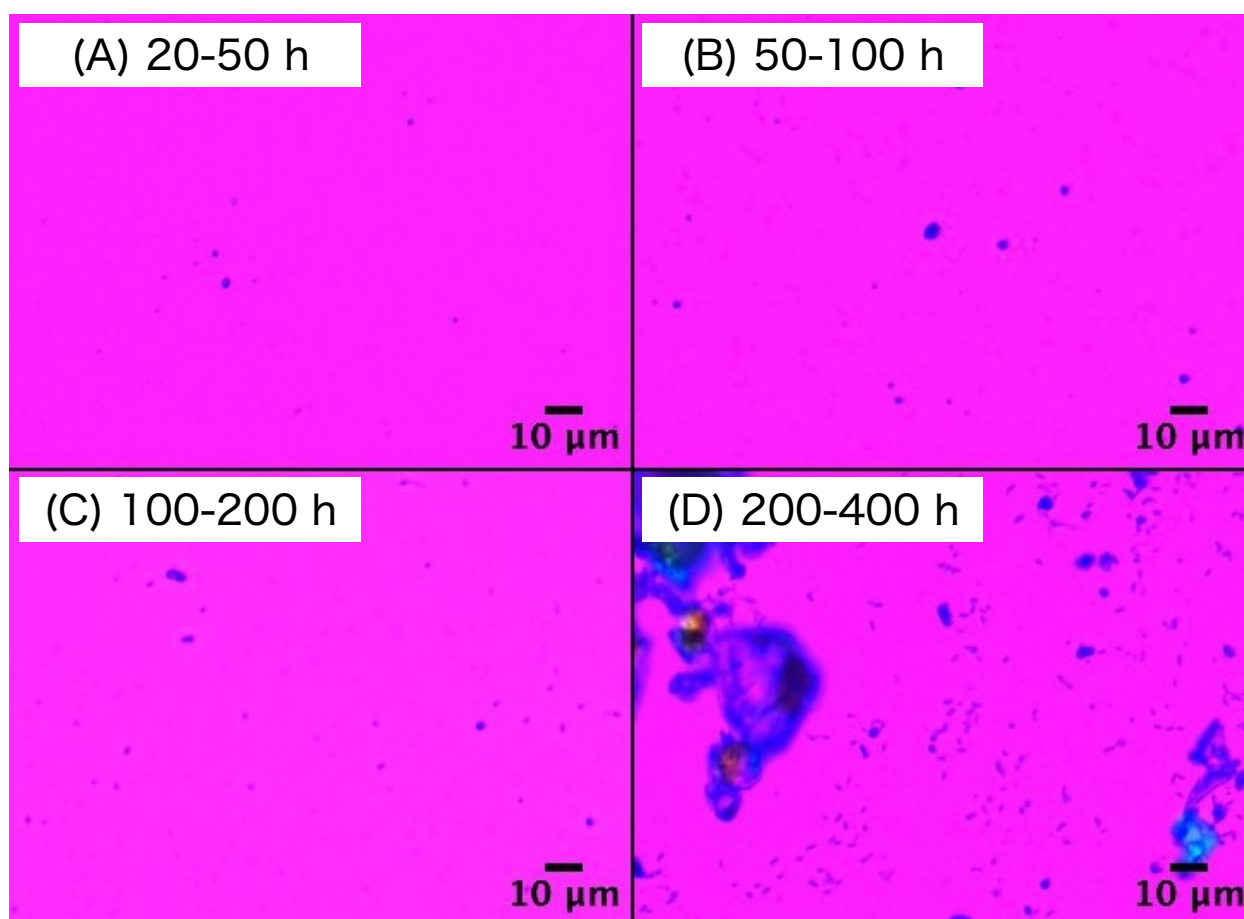


Figure 1 (A-D) Polarized optical microscope images of MPs fragmented from photo-aged PP specimens after more than 20 h of stirring.

3.2 Evolution of MP Size Distribution

Figure 2 shows the size distributions of MPs at each stirring period (20–50 h, 50–100 h, 100–200

h, and 200–400 h) plotted in linear, semi-logarithmic, and double-logarithmic manners. MPs were not observed by the optical microscope at the early stage (less than about 20 h of stirring). Thus, only the data after 20 h of stirring are shown in Figure 2. The functional form of the MP size distributions qualitatively changed with the stirring time. The MP size distributions for 20–50 h and 50–100 h exhibited an exponential dependence $P(x) \propto \exp(-x/x_0)$. Here, x is the MP size, $P(x)$ is the distribution, and x_0 is a constant. x_0 can be interpreted as a characteristic MP size. In contrast, the MP size distributions for 100–200 h and 200–400 h exhibited a power-law dependence $P(x) \propto x^{-\alpha}$, where α is the exponent. Unlike the exponential distribution, the power-law distribution has no characteristic size. The power-law exponents observed in Figure 2C are 3.3 for 100–200 h and 3.2 for 200–400 h, which are close to but somewhat larger than the exponent of 3 expected for a purely random 3D fragmentation model [23].

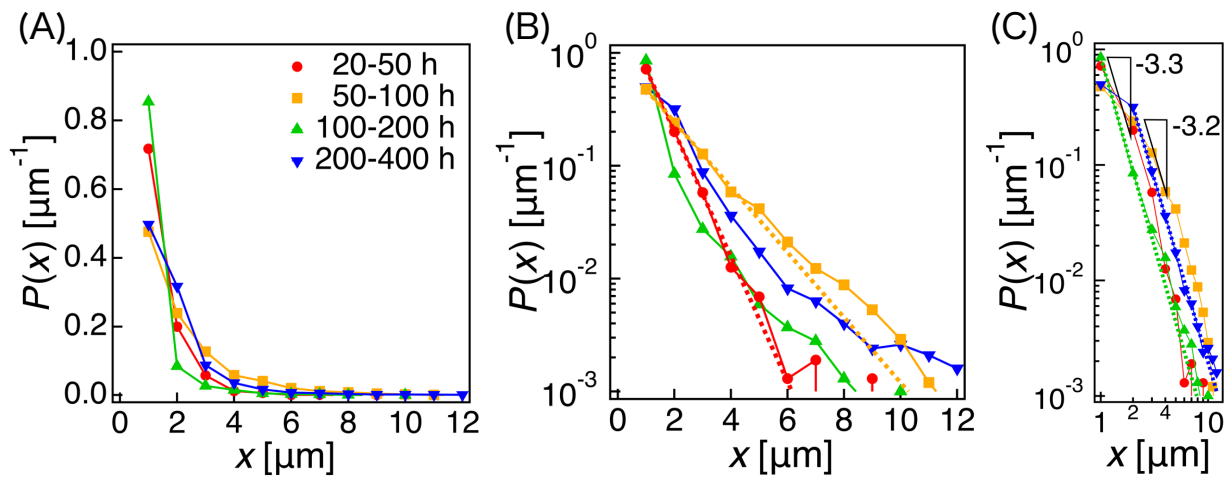


Figure 2 MP size distributions at each stirring period plotted on (A) linear, (B) semi-logarithmic, and (C) logarithmic scales. The MP size distributions for 20–50 h and 50–100 h exhibited an exponential dependence, $P(x) \propto \exp(-x/x_0)$ (lines in (B)), while the MP size distributions for 100–200 h and 200–400 h exhibited a power-law dependence, $P(x) \propto x^{-\alpha}$ (lines in (C)). The characteristic MP sizes x_0 for 20–50 h and 50–100 h were 0.67 μm and 1.3 μm , respectively. The power-law exponents α for 100–200 h and 200–400 h were 3.3 and 3.2, respectively.

3.3 Fragmentation Rate of MPs and NPs

Figure 3 shows the average fragmentation rate ($R_{\text{frag},i}$) and the accumulated weight ($W_{\text{frag},n}$) of MPs and NPs as functions of stirring time. The average fragmentation rate decreased sharply until 20 h of stirring, reached a minimum at 20 h, and then slightly increased. At the longer stirring time, it started to decrease again. Here, note that $R_{\text{gen},i}$ is the average value in the i -th stirring period, and the stirring period is not constant. The local minimum at $t_i = 20$ h may not be accurate, and it is not discussed further in what follows. After 400 h of stirring, about 1.4 mg MPs were fragmented from the specimen. The weight of unaged specimens was about 0.8 g, indicating that 1/500 of the specimen fragmented into MPs.

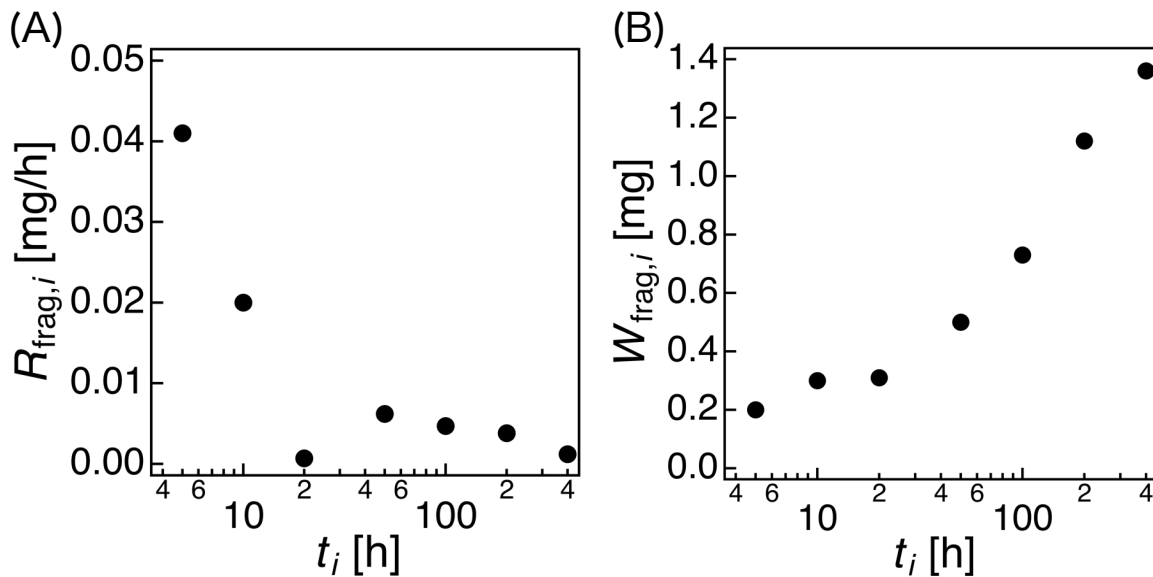


Figure 3 Time evolution of (A) the average fragmentation rate of MPs and NPs and (B) the accumulated weight of fragmented MPs and NPs. t_i is end of the i -th stirring period.

3.4 Observation of Remaining PP Specimen Surface

Optical microscope images of the photo-aged PP specimen surface after different stirring times are shown in Figure 4. Even without stirring, surface embrittlement occurred during the photo-aging process, and spontaneous cracks could be observed on the specimen surface (Figure 4A), as reported earlier [15,16]. The distance between neighboring cracks was about 100–200 μm [32,33]. Some cracks were connected in a pattern resembling a capital letter "T" known as the formation of T-

junction [34,35], consistent with chemi-crystallization-induced crack propagation [25,26]. Surrounded by these cracks, island-like regions on the surface of the photo-aged specimen were formed. For the stirring time of 5–200 h, in addition to the island-like regions, some narrow cracks were observed inside them. These narrow cracks were probably formed by the mechanical stresses (See Figures 4B–4G). According to the results in Figure 3, traces of MP fragmentation are expected to be observed. Indeed, compared with Figure 4A, edges formed by cracks appear more obscure. After the photo-aged specimen was stirred for 400 h (Figure 4H), mesh-like cracks and some spots with the fragmentation of MPs were observed inside the island-like regions. Also, warp along cracks was observed in Figure 4B–4H.

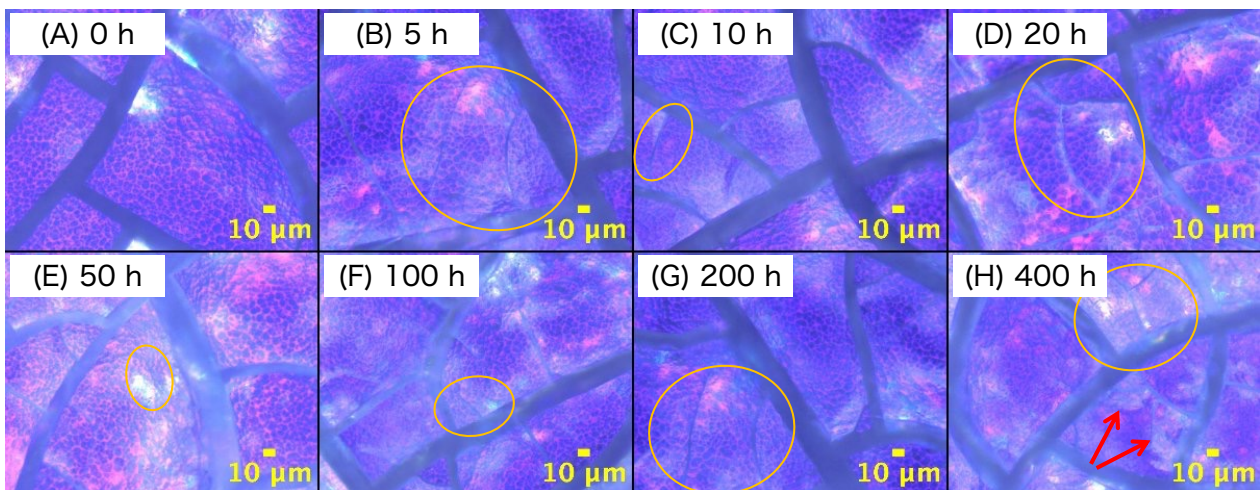


Figure 4 (A-H) Polarized optical microscope images of specimen surface after stirring for 0 h to 400 h. The locations where MPs fragmented in Figure 4H are highlighted by the red arrows. Circles show cracks in the island-like regions.

Figure 5 shows a mapping image of the orientation parameter R and a polarized optical microscope image of the unaged PP specimen. Spherulites were observed, and the spherulite size was approximately 30 μm .

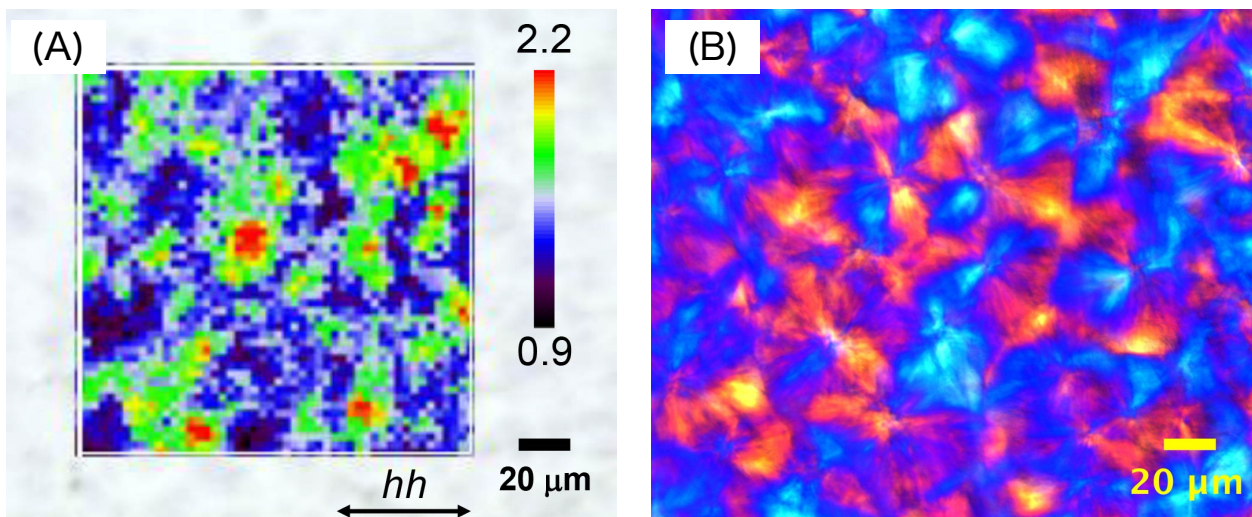


Figure 5 (A) Mapping image of the orientation parameter R and (B) polarized optical microscope image of the unaged PP specimen.

3.5 Physico-Chemical Analysis in The Process of MP Fragmentation

The IR spectra of the PP specimens unaged, photo-aged, and stirred for 400 h after photo-aging are shown in Figure 6. IR spectra were normalized by the area of peak at 1458 cm^{-1} , which corresponds to the asymmetric CH_3 bending mode [36]. Upon photo-aging, the absorbance in the $1800\text{--}1700\text{ cm}^{-1}$ region increases significantly. These peaks in this region are attributed to $\text{C}=\text{O}$ vibrations, and the change is associated with the formation of end-group carboxylic acids at 1712 cm^{-1} and ester structures at 1735 cm^{-1} [47]. These are low-molecular-weight oxygenated products. In the IR spectrum obtained after 400 h of stirring, the absorbance for the $\text{C}=\text{O}$ peaks decreased, reflecting the dissolution of photo-oxidized products as soluble components into water.

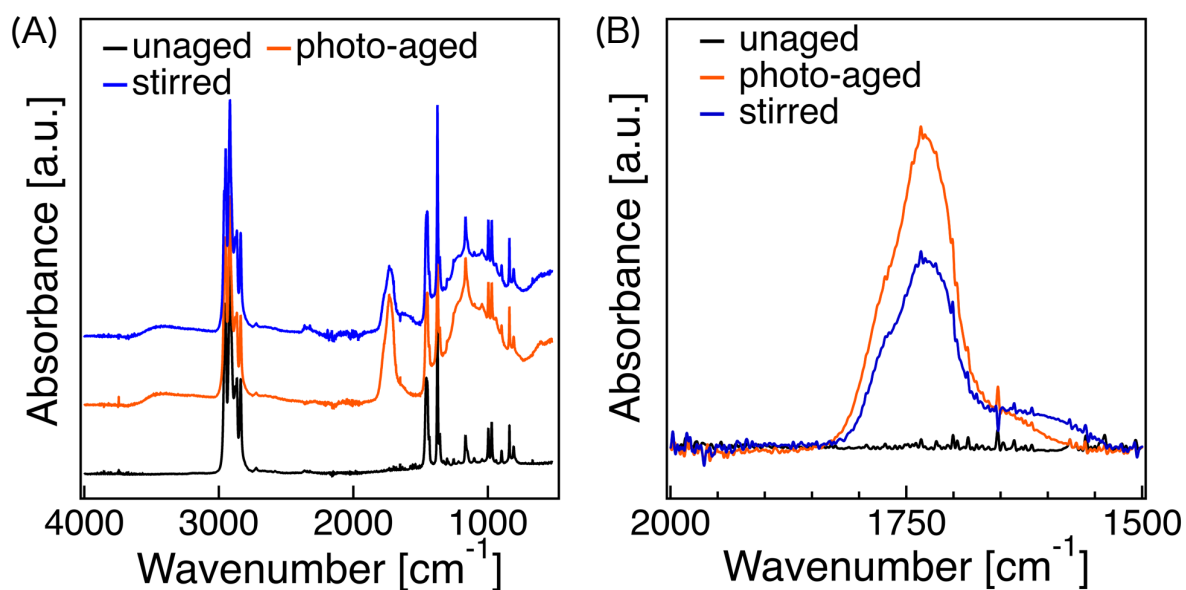


Figure 6 IR spectra of the specimen unaged, photo-aged, and stirred for 400 h after photo-aging in the regions of (A) 4000–400 cm^{-1} and (B) 2000–1500 cm^{-1} normalized by the area of the peak at 1458 cm^{-1} . The IR spectra in (B) are corrected for baseline.

Figure 7 shows the DSC traces of the PP specimens unaged, photo-aged, and stirred for 400 h after photo-aging. One can see a shift of the melting peak to the lower temperature region induced by the photo-aging. In addition, the peak shape changes, implying multiple overlapping peaks. Such behavior triggered by photo-aging has been frequently observed in earlier studies [37–39]. This result suggests the formation of low- T_m (i.e., smaller) crystals due to the change in crystalline structures. Photo-aging induces chain scission, which subsequently triggers chemi-crystallization. These processes likely lead to damage of the crystalline lamellae and fragmentation of the crystalline regions. The enthalpies of fusion of the PP specimens unaged, photo-aged, and stirred for 400 h after photo-aging were 80 J/g, 86 J/g, and 84 J/g, respectively. The crystallinity clearly increases upon photo-aging, most likely reflecting the contribution of chemi-crystallization. In contrast, the stirring did not significantly alter the DSC curve and the crystallinity.

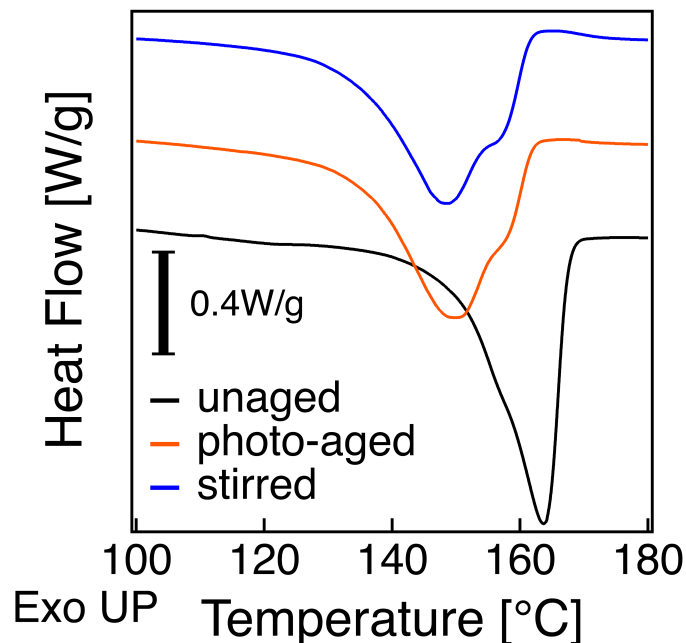


Figure 7 DSC traces of the PP specimens unaged, photo-aged, and stirred for 400 h after photo-aging.

Figure 8 shows the Raman spectra at the spots in the PP specimens unaged, photo-aged, and stirred for 400 h after photo-aging. For comparison, the Raman spectrum of a MP is also shown. All Raman spectra were normalized by the area of the peak at 1440 cm^{-1} , which serves as an internal standard insensitive to photo-aging [39]. The peak at 810 cm^{-1} corresponds to consecutive helical C–C backbone chains with more than 12 monomers terminated by $-\text{CH}_3$, while the peak at 830 cm^{-1} is attributed to amorphous backbone chains. The peaks at 830 cm^{-1} and 841 cm^{-1} are associated with amorphous and short helical backbone chains, respectively [40]. The Raman spectra were fitted to a sum of three Voigt functions (See Figure S1 in the Supporting Information), and peak areas of three peaks were calculated. Then the crystallinities of specimens and a MP were calculated as:

$$\chi = \frac{A_{810}}{A_{810} + A_{830} + A_{841}}. \quad (3)$$

Here, A_{810} , A_{830} , and A_{841} are the peak areas for the peaks located around 810 cm^{-1} , 830 cm^{-1} , and 841 cm^{-1} , respectively. It was assumed that the chains in crystalline regions have sufficiently long helical sequences. The calculated crystallinities are shown in Figure 8B. The photo-aged PP specimen

exhibits higher crystallinity than the unaged specimen, implying chemi-crystallization, consistent with the DSC (Figure 7). The high crystallinity of the MP and the low crystallinity of the remaining specimen imply that high crystallinity regions are preferentially fragmented into MPs. In addition, the crystallinity remarkably differs spot to spot for the specimens stirred for 400 h after photo-aging. The spot where MP fragmentation occurred exhibited lower crystallinity than that without the fragmentation.

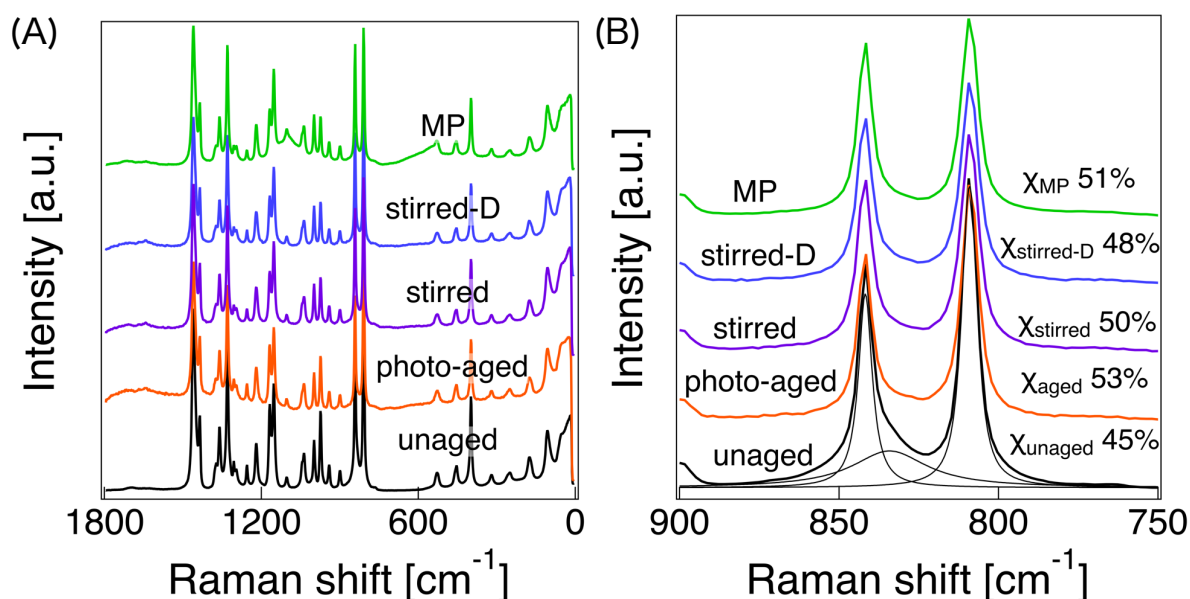


Figure 8 Raman spectra of an unaged specimen, a photo-aged specimen, several spots of the stirred specimen for 400 h after photo-aging, and an MP fragmented after photo-aging followed by 400 h of stirring, in the regions of (A) 1800–0 cm^{-1} and (B) 900–750 cm^{-1} normalized by the area of the peak at 1440 cm^{-1} . Spots of the stirred specimen with and without the fragmentation of MPs were labeled as “stirred” and “stirred-D”, respectively. The crystallinity at each spot is shown in (B).

4. DISCUSSION

In this section, from the experimental results shown above, let us discuss the MP formation process under stirring. Just after photo-aging (before stirring), deep cracks appear on the surface of the PP specimen (Figure 4A) due to chemi-crystallization, which causes embrittlement of the specimen.

Between 0 and 20 h of stirring, MPs were not observed, while the fragmentation of MPs and NPs was observed as an increase in the weight of collected particles (Figure 3) with the presence of a waxy residue. This observation suggests the initial fragmentation of NP ($< 1 \mu\text{m}$) components. Also, mechanical stress and immersion in water may cause the formation of new cracks [41] and promote crack propagation. This crack propagation may induce MPs ($> 1 \mu\text{m}$) fragmentation after 20 h of stirring.

Between 20 and 100 h of stirring, MPs ($> 1 \mu\text{m}$) were fragmented. Compared to Figure 4A, the edges formed by cracks appear more obscure in Figure 4D-4F, implying that MPs may be fragmented through a process in which sharp edges gradually round off. When a mechanical stress is applied to a photo-aged specimen, stress concentration will occur at the crack propagation front. In addition, the oxidation is promoted around cracks [42]. The regions around the edges might be selectively damaged.

In this period, the MP size distribution followed an exponential distribution (Figure 2). No prior reports highlight such a behavior. The reason for this exponential distribution remains unclear, but the fact that an exponential distribution is realized implies the existence of a characteristic length scale which governs the MP fragmentation. One might expect that such a characteristic size is related to hierarchical crystalline structures of PP. However, the spherulite size of PP estimated by a micro-Raman imaging and a polarized optical microscope image was approximately $30 \mu\text{m}$ (Figure 5). Almost all observed MPs were smaller than the spherulites. Further investigation is required to determine on this issue.

Between 100 and 400 h of stirring, larger MPs ($> 10 \mu\text{m}$) were fragmented, and the MP size distribution shifted to power-law distributions (Figure 2). This power-law distribution is consistent with previous reports [11,17,20–26]. No earlier studies have documented the transition of MP size distribution with increasing stirring time. The observed transition probably reflects a change in the MP fragmentation mechanism. A power-law distribution often arises from some scale-free, fractal processes. Although the detailed mechanism is not clear, it is expected that the MP formation process has some fractal natures. The power-law exponents in our data are about 3.2, which is somewhat

larger than the commonly reported value of 3. The exponent of 3 is often attributed to the 3D fragmentation model [23], but our data imply that the 3D fragmentation model may not fully explain the MP fragmentation behavior. The origin of the power-law exponent may not be the cascaded fragmentation, but some fractal structures at the surface of photo-aged plastics. For example, propagation pathways of cracks may have a fractal shape. Then the size distribution of MPs fragmented along propagated cracks will reflect the fractal nature.

The MP fragmentation from the photo-aged PP specimen surface is also supported by spectroscopic data (IR and Raman spectra). The IR spectra imply that the chemi-crystallized regions on the surface decrease with stirring. The Raman spectra suggest that the crystallinity of the surface decreases after the fragmentation. These results are consistent with the scenario that chemi-crystallized surface regions are damaged and fragmented into MPs by stirring. UV irradiation significantly affects the surface region, but the bulk region is not largely affected [43]. At the very long stirring times, the depth dependence of crystallinity may become important.

5. CONCLUSION

The time evolution of MP size distribution and the fragmentation rate of MPs and NPs during the stirring process of photo-aged PP specimens were investigated. MPs were fragmented from the photo-aged PP specimen by stirring in deionized water. During the stirring, the size of the fragmented MPs increased with increasing stirring time, and the size distribution transitioned from an exponential to a power-law distribution. Also, the fragmentation rate decreased steeply at the early stage before gradually decreasing at longer stirring times. IR and Raman spectroscopy revealed that MPs were fragments of high crystallinity regions at the specimen surface. The proposed scenario for MP fragmentation is as follows: High crystallinity regions are formed at the surface during the photo-aging process. The surface region becomes brittle, and cracks form. During the stirring, additional cracks are formed and propagated. Eventually, the high crystallinity regions are fragmented along the surface cracks and released as MPs.

Author Information

Corresponding Authors

Takato Ishida - Department of Materials Physics, Nagoya University, Furo-cho, Chikusa, Nagoya 464-8601, Japan; orcid. Org/0000-0003-3919-2348; E-mail: ishida@mp.pse.nagoya-u.ac.jp

Authors

Kazuya Haremaki - Department of Materials Physics, Nagoya University, Furo-cho, Chikusa, Nagoya 464-8603, Japan; orcid. Org/0009-0007-8494-8008; E-mail: haremaki.kazuya.w2@s.mail.nagoya-u.ac.jp

Takumitsu Kida - Department of Materials Chemistry, Faculty of Engineering, The University of Shiga Prefecture, 2500, Hassaka, Hikone, 522-8533, Japan; orcid. Org/0000-0002-9494-3004

Yusuke Koide - Department of Materials Physics, Nagoya University, Furo-cho, Chikusa, Nagoya 464-8603, Japan; orcid. Org/0000-0002-4843-6888; E-mail: koide.yusuke.k1@f.mail.nagoya-u.ac.jp

Takashi Uneyama - Department of Materials Physics, Nagoya University, Furo-cho, Chikusa, Nagoya 464-8603, Japan; orcid. Org/0000-0001-6607-537X; E-mail: uneyama@mp.pse.nagoya-u.ac.jp

Yuichi Masubuchi - Department of Materials Physics, Nagoya University, Furo-cho, Chikusa, Nagoya 464-8603, Japan; orcid. Org/0000-0002-1306-3823; E-mail: mas@mp.pse.nagoya-u.ac.jp

Conflict of Interest

The authors declare no competing interests.

Acknowledgment

This work was supported by JSPS KAKENHI Grant Numbers 24K20949, 22KJ1543, "Nagoya University High Performance Computing Research Project for Joint Computational Science" in Japan,

CCI holdings Co., Ltd., Mayekawa Houonkai Foundation, Suzuki Foundation, Yazaki Memorial Foundation for Science and Technology, Fujimori Science and Technology Foundation, Fuji Seal Foundation, The Naito Research Grant and Suga Weathering Technology Foundation, JST PRESTO Grant Number JPMJPR23N3, Japan.

References

- [1] J.P.G.L. Frias, R. Nash, Microplastics: Finding a consensus on the definition, *Marine Pollution Bulletin* 138 (2019) 145–147. <https://doi.org/10.1016/j.marpolbul.2018.11.022>.
- [2] A.L. Lusher, V. Tirelli, I. O'Connor, R. Officer, Microplastics in Arctic polar waters: the first reported values of particles in surface and sub-surface samples, *Sci Rep* 5 (2015) 14947. <https://doi.org/10.1038/srep14947>.
- [3] J. Li, H. Liu, J. Paul Chen, Microplastics in freshwater systems: A review on occurrence, environmental effects, and methods for microplastics detection, *Water Research* 137 (2018) 362–374. <https://doi.org/10.1016/j.watres.2017.12.056>.
- [4] S. Eo, S.H. Hong, Y.K. Song, G.M. Han, S. Seo, W.J. Shim, Prevalence of small high-density microplastics in the continental shelf and deep sea waters of East Asia, *Water Research* 200 (2021) 117238. <https://doi.org/10.1016/j.watres.2021.117238>.
- [5] Y. Zhang, S. Kang, S. Allen, D. Allen, T. Gao, M. Sillanpää, Atmospheric microplastics: A review on current status and perspectives, *Earth-Science Reviews* 203 (2020) 103118. <https://doi.org/10.1016/j.earscirev.2020.103118>.
- [6] M.C. Rillig, A. Lehmann, Microplastic in terrestrial ecosystems, *Science* 368 (2020) 1430–1431. <https://doi.org/10.1126/science.abb5979>.
- [7] K.L. Law, R.C. Thompson, Microplastics in the seas, *Science* 345 (2014) 144–145. <https://doi.org/10.1126/science.1254065>.
- [8] K. Tanaka, H. Takada, Microplastic fragments and microbeads in digestive tracts of planktivorous fish from urban coastal waters, *Sci Rep* 6 (2016) 34351. <https://doi.org/10.1038/srep34351>.
- [9] Y. Yang, E. Xie, Z. Du, Z. Peng, Z. Han, L. Li, R. Zhao, Y. Qin, M. Xue, F. Li, K. Hua, X. Yang, Detection of Various Microplastics in Patients Undergoing Cardiac Surgery, *Environ. Sci. Technol.* 57 (2023) 10911–10918. <https://doi.org/10.1021/acs.est.2c07179>.
- [10] A. Isobe, K. Kubo, Y. Tamura, S. Kako, E. Nakashima, N. Fujii, Selective transport of microplastics and mesoplastics by drifting in coastal waters, *Marine Pollution Bulletin* 89 (2014) 324–330. <https://doi.org/10.1016/j.marpolbul.2014.09.041>.
- [11] A. Ter Halle, L. Ladirat, X. Gendre, D. Goudouneche, C. Pusineri, C. Routaboul, C.

- Tenailleau, B. Duployer, E. Perez, Understanding the Fragmentation Pattern of Marine Plastic Debris, *Environ. Sci. Technol.* 50 (2016) 5668–5675. <https://doi.org/10.1021/acs.est.6b00594>.
- [12] B. Fayolle, L. Audouin, J. Verdu, Oxidation induced embrittlement in polypropylene D a tensile testing study, *Polymer Degradation and Stability* (2000).
- [13] B. Fayolle, L. Audouin, J. Verdu, A critical molar mass separating the ductile and brittle regimes as revealed by thermal oxidation in polypropylene, *Polymer* 45 (2004) 4323–4330. <https://doi.org/10.1016/j.polymer.2004.03.069>.
- [14] C. Rouillon, P.-O. Bussiere, E. Desnoux, S. Collin, C. Vial, S. Therias, J.-L. Gardette, Is carbonyl index a quantitative probe to monitor polypropylene photodegradation?, *Polymer Degradation and Stability* 128 (2016) 200–208. <https://doi.org/10.1016/j.polymdegradstab.2015.12.011>.
- [15] I. Yakimets, D. Lai, M. Guigon, Effect of photo-oxidation cracks on behaviour of thick polypropylene samples, *Polymer Degradation and Stability* 86 (2004) 59–67. <https://doi.org/10.1016/j.polymdegradstab.2004.01.013>.
- [16] G.E. Schoolenberg, A fracture mechanics approach to the effects of UV-degradation on polypropylene, *J Mater Sci* 23 (1988) 1580–1590. <https://doi.org/10.1007/BF01115695>.
- [17] Y.K. Song, S.H. Hong, S. Eo, W.J. Shim, Fragmentation of nano- and microplastics from virgin- and additive-containing polypropylene by accelerated photooxidation, *Environmental Pollution* 327 (2023) 121590. <https://doi.org/10.1016/j.envpol.2023.121590>.
- [18] F. Julienne, N. Delorme, F. Lagarde, From macroplastics to microplastics: Role of water in the fragmentation of polyethylene, *Chemosphere* 236 (2019) 124409. <https://doi.org/10.1016/j.chemosphere.2019.124409>.
- [19] N. Kalogerakis, K. Karkanorachaki, G.C. Kalogerakis, E.I. Triantafyllidi, A.D. Gotsis, P. Partsinevelos, F. Fava, Microplastics Generation: Onset of Fragmentation of Polyethylene Films in Marine Environment Mesocosms, *Front. Mar. Sci.* 4 (2017). <https://doi.org/10.3389/fmars.2017.00084>.
- [20] M. Kooi, S. Primpke, S.M. Mintenig, C. Lorenz, G. Gerds, A.A. Koelmans, Characterizing the multidimensionality of microplastics across environmental compartments, *Water Research* 202 (2021) 117429. <https://doi.org/10.1016/j.watres.2021.117429>.
- [21] Y.K. Song, S.H. Hong, M. Jang, G.M. Han, S.W. Jung, W.J. Shim, Combined Effects of UV Exposure Duration and Mechanical Abrasion on Microplastic Fragmentation by Polymer Type, *Environ. Sci. Technol.* 51 (2017) 4368–4376. <https://doi.org/10.1021/acs.est.6b06155>.
- [22] R. Lenz, K. Enders, T.G. Nielsen, Microplastic exposure studies should be environmentally realistic, *Proc. Natl. Acad. Sci. U.S.A.* 113 (2016). <https://doi.org/10.1073/pnas.1606615113>.
- [23] A. Cózar, F. Echevarría, J.I. González-Gordillo, X. Irigoien, B. Ubeda, S. Hernández-León, A.T. Palma, S. Navarro, J. García-de-Lomas, A. Ruiz, M.L. Fernández-de-Puelles, C.M. Duarte, Plastic debris in the open ocean, *Proc Natl Acad Sci U S A* 111 (2014) 10239–10244. <https://doi.org/10.1073/pnas.1314705111>.
- [24] A. Cózar, M. Sanz-Martín, E. Martí, J.I. González-Gordillo, B. Ubeda, J.Á. Gálvez, X. Irigoien, C.M. Duarte, Plastic Accumulation in the Mediterranean Sea, *PLoS ONE* 10 (2015)

e0121762. <https://doi.org/10.1371/journal.pone.0121762>.

- [25] C. Sorasan, C. Edo, M. González-Pleiter, F. Fernández-Piñas, F. Leganés, A. Rodríguez, R. Rosal, Ageing and fragmentation of marine microplastics, *Science of The Total Environment* 827 (2022) 154438. <https://doi.org/10.1016/j.scitotenv.2022.154438>.
- [26] K. Aoki, R. Furue, A model for the size distribution of marine microplastics: A statistical mechanics approach, *PLoS ONE* 16 (2021) e0259781. <https://doi.org/10.1371/journal.pone.0259781>.
- [27] J. Martin, P. Bourson, A. Dahoun, J.M. Hiver, The β -Spherulite Morphology of Isotactic Polypropylene Investigated by Raman Spectroscopy, *Appl Spectrosc* 63 (2009) 1377–1381. <https://doi.org/10.1366/000370209790109067>.
- [28] S. Lambert, M. Wagner, Formation of microscopic particles during the degradation of different polymers, *Chemosphere* 161 (2016) 510–517. <https://doi.org/10.1016/j.chemosphere.2016.07.042>.
- [29] K. Enders, R. Lenz, C.A. Stedmon, T.G. Nielsen, Abundance, size and polymer composition of marine microplastics $\geq 10 \mu\text{m}$ in the Atlantic Ocean and their modelled vertical distribution, *Marine Pollution Bulletin* 100 (2015) 70–81. <https://doi.org/10.1016/j.marpolbul.2015.09.027>.
- [30] P.L. Corcoran, M.C. Biesinger, M. Grifi, Plastics and beaches: A degrading relationship, *Marine Pollution Bulletin* 58 (2009) 80–84. <https://doi.org/10.1016/j.marpolbul.2008.08.022>.
- [31] F. Julienne, F. Lagarde, N. Delorme, Influence of the crystalline structure on the fragmentation of weathered polyolefines, *Polymer Degradation and Stability* 170 (2019) 109012. <https://doi.org/10.1016/j.polymdegradstab.2019.109012>.
- [32] Y. An, T. Kajiwara, A. Padermshoke, T.V. Nguyen, S. Feng, H. Masunaga, Y. Kobayashi, H. Ito, S. Sasaki, A. Isobe, A. Takahara, Photooxidative degradation and fragmentation behaviors of oriented isotactic polypropylene, *Polym J* 56 (2024) 379–389. <https://doi.org/10.1038/s41428-023-00876-4>.
- [33] E. Kuka, D. Cirule, I. Andersone, L.O. Vasiljevs, J. Merna, A. Sarakovskis, N. Kurnosova, E. Sansonetti, L. Vevere, B. Andersons, A step to microplastic formation: Microcracking and associated surface transformations of recycled LDPE, LLDPE, HDPE, and PP plastics exposed to UV radiation, *Polymer Degradation and Stability* 229 (2024) 110967. <https://doi.org/10.1016/j.polymdegradstab.2024.110967>.
- [34] S. Kitsunozaki, Crack growth in drying paste, *Advanced Powder Technology* 22 (2011) 311–318. <https://doi.org/10.1016/j.appt.2011.03.006>.
- [35] L. Goehring, S.W. Morris, Cracking mud, freezing dirt, and breaking rocks, *Physics Today* 67 (2014) 39–44. <https://doi.org/10.1063/PT.3.2584>.
- [36] J. Zhao, Z. Peng, J. Zhang, G. Li, In situ FT-IR spectroscopy study on the conformational changes of quenched isotactic polypropylene during stepwise heating, *Polym. Bull.* 67 (2011) 1649–1659. <https://doi.org/10.1007/s00289-011-0556-2>.
- [37] J. Guisández, P. Tiemblo, J.M. Gómez-Elvira, Change of thermal and dynamic-mechanical behaviour of a metallocene isotactic polypropylene during low-temperature thermo-oxidation, *Polymer Degradation and Stability* 87 (2005) 543–553. <https://doi.org/10.1016/j.polymdegradstab.2004.10.014>.

- [38] B. Fayolle, E. Richaud, X. Colin, J. Verdu, Review: degradation-induced embrittlement in semi-crystalline polymers having their amorphous phase in rubbery state, *J Mater Sci* 43 (2008) 6999–7012. <https://doi.org/10.1007/s10853-008-3005-3>.
- [39] T. Kida, M. Yamaguchi, Role of Rigid–Amorphous chains on mechanical properties of polypropylene solid using DSC, WAXD, SAXS, and Raman spectroscopy, *Polymer* 249 (2022) 124834. <https://doi.org/10.1016/j.polymer.2022.124834>.
- [40] R.M. Khafagy, *In situ* FT-Raman spectroscopic study of the conformational changes occurring in isotactic polypropylene during its melting and crystallization processes, *J Polym Sci B Polym Phys* 44 (2006) 2173–2182. <https://doi.org/10.1002/polb.20891>.
- [41] J.-F. Larché, P.-O. Bussière, J.-L. Gardette, How to reveal latent degradation of coatings provoked by UV-light, *Polymer Degradation and Stability* 95 (2010) 1810–1817. <https://doi.org/10.1016/j.polymdegradstab.2010.05.005>.
- [42] M.L. Castejón, P. Tiemblo, J.M. Gómez-Elvira, Photo-oxidation of thick isotactic polypropylene films I. Characterisation of the heterogeneous degradation kinetics, *Polymer Degradation and Stability* 70 (2000) 357–364. [https://doi.org/10.1016/S0141-3910\(00\)00123-3](https://doi.org/10.1016/S0141-3910(00)00123-3).
- [43] N. Nagai, T. Matsunobe, T. Imai, Infrared analysis of depth profiles in UV-photochemical degradation of polymers, *Polymer Degradation and Stability* 88 (2005) 224–233. <https://doi.org/10.1016/j.polymdegradstab.2004.11.001>.

Supporting Information

Effects of Stirring Time on Formation of Microplastics Fragmented from Photo-aged Polypropylene

Kazuya Haremake^a, Takumitsu Kida^b, Yusuke Koide^a,

Takashi Uneyama^a, Yuichi Masubuchi^a, Takato Ishida^{a}*

^a Department of Materials Physics, Nagoya University, Furo-cho, Chikusa, Nagoya 464-8603, Japan

^b Department of Materials Chemistry, Faculty of Engineering, The University of Shiga Prefecture, 2500, Hassaka, Hikone, 522-8533, Japan

Tel: +81-52-789-4202, Mobile:+81-90-1145-4372

E-mail address: ishida@mp.pse.nagoya-u.ac.jp

TABLE OF CONTENTS

1. **Raman spectra analysis** ----- S3

1. Raman spectra analysis

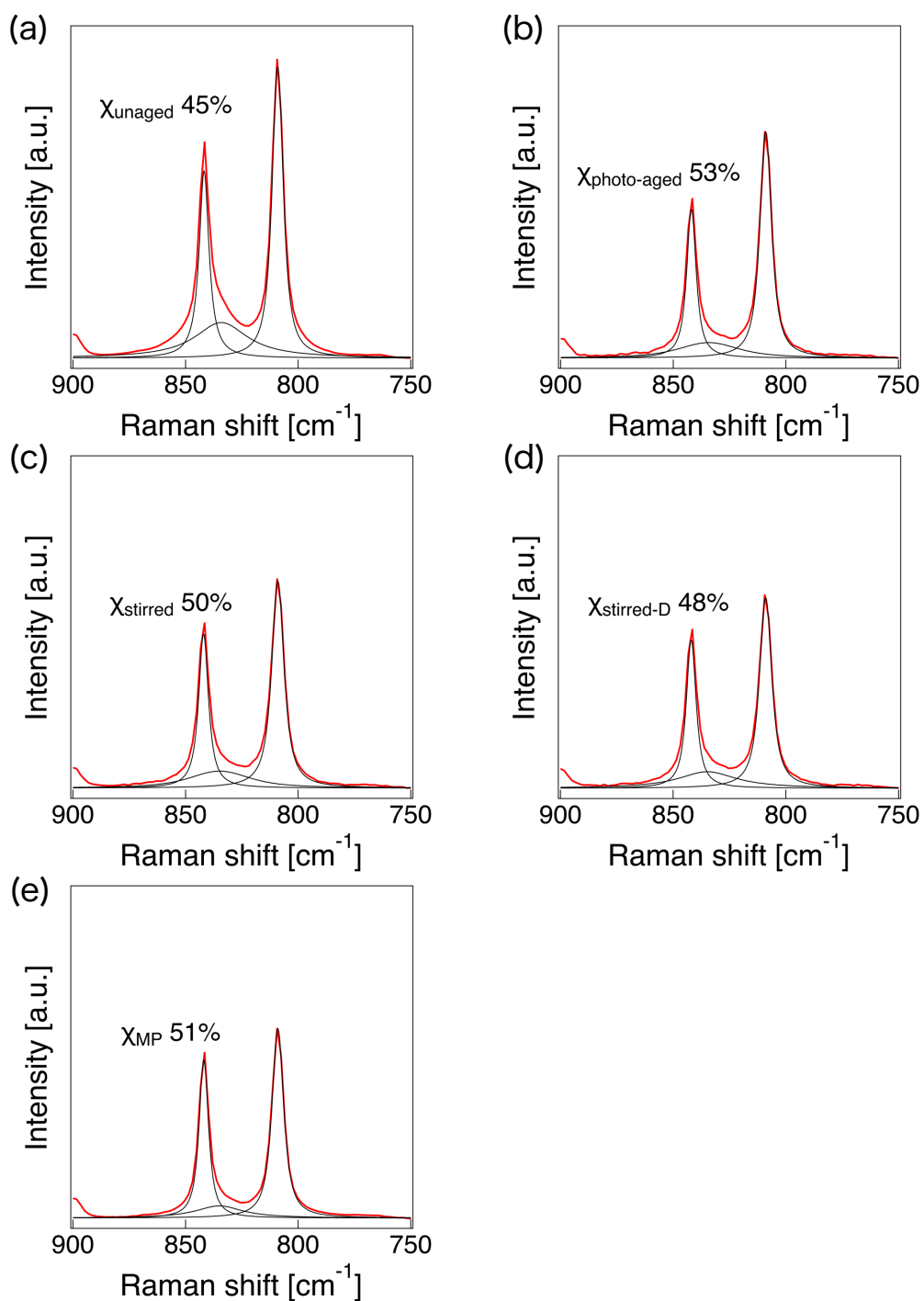


Figure S1 Raman spectra for 900-750 cm^{-1} and peak fitting results of (a) unaged, (b) photo-aged, (c) stirred, (d) stirred-D, (e) MP samples. Spots of the stirred specimen with and without the fragmentation of MPs were referred to as “stirred” and “stirred-D”, respectively. Thin black curves represent the peak fitting results with three Voigt functions.